PASSIVE VHF RADAR INTERFEROMETER OBSERVATION OF METEOR TRAILS

Melissa Meyer[1], **Chucai Zhou**[2], **Dawn Gidner**[3], **John Sahr**[4]

[1] ***University of Washington, Electrical Engineering, Box 352500 Seattle WA, 98195-2500, USA***
Tel: +1-206-221-6513, Fax: +1-206-543-3842, Email: mgmeyer@u.washington.edu
[2] ***As (1) above, but Email: chucai@rcs.ee.washington.edu***
[3] ***As (1) above, but Email: dawn@u.washington.edu***
[4] ***As (1) above, but Tel: +1-206-685-4816, Email: jdsahr@ee.washington.edu***

ABSTRACT

In recent years, we have demonstrated a passive VHF radar technique for studying the high latitude ionosphere. This technique produces Doppler power spectrum as a function of range, with high range, time, and Doppler resolution. Here we describe the addition of interferometric capability to passive radar technique employed at the Manastash Ridge Radar, a passive, bistatic system which observes commercial FM broadcasts at 100 MHz. We discuss the implementation of an interferometer for passive radar and present initial observations of ground clutter, airplanes, and meteors, as well as very early results for auroral E-region irregularities. In particular, we show an azimuthal angular resolution of 0.1° with a 70 meter antenna baseline, for a meteor at 800 km range.

INTRODUCTION

The Manastash Ridge Radar (MRR) is a passive, bistatic radar which detects the scatter of commercial FM radio broadcasts in order to observe ionospheric plasma density irregularities [3, 1]. It offers superb range and Doppler resolution at a wavelength between those at 50 and 140 MHz. The sensitivity and range/Doppler resolution are comparable or superior to conventional coherent radars. In this paper, we extend the passive radar technique to include interferometry, thus permitting the estimation of transverse structure in addition to the range distribution. Thus, the passive radar technique provides data sets which are functionally equivalent to conventional active radar interferometers [2], and to whose data ours may be directly compared.

By fortunate coincidence, FM broadcasts provide useful illumination for studies of scattering in the ionosphere. The meter scale wavelength scatters readily from ionospheric density irregularities and meteor trails, yet suffers little refraction. The average power is comparable to that provided by dedicated instruments, and the typical broadcast waveform has a superb ambiguity function in the average sense, completely free of range and doppler aliasing. FM broadcasts have much greater bandwidth than the fluctuations of the ionospheric plasma, and this permits overspread target pulse compression for unambiguous estimation of the target correlation function.

In order to recover the data, we must correlate the scattered signal with the broadcast signal. Rather than attempt to separate the direct and scattered signals in a single receiver, we place one receiver near the transmitter to provide a reference. A second receiver is located far away, behind a mountain range, so it is exposed primarily to the scattered signal — drastically lowering the dynamic range required of the receivers. A system diagram is illustrated in Fig. 1.

SIGNAL PROCESSING

To extract the interferometric information, we pursue the suggestion for interferometry made by Sahr and Lind [3]. First, we denote the signal arising from the transmitter as $x(t)$, and scattered signals in the remote receivers are similarly denoted $y_n(t)$, where n indicates a particular antenna in the interferometric array. For the purpose of this report, we will assume that the scattered signals $y_n(t)$ are completely free of "direct" illumination ($x(t)$). In practice, this is only partially true; techniques to ameliorate direct path and ground clutter pollution are discussed elsewhere by [4] (this meeting).

Our signal processing algorithm first performs a coherent, partial correlation (essentially a matched filter operation):

$$z_n(r;\bar{t}) = \int_{\bar{t}}^{\bar{t}+T} y_n(t)x^*(t-2r/c)\,dt \tag{1}$$

The signal $z_n(r;\bar{t})$ is a time series of the scatterer which evolves at the low bandwidth rate of the scatterer (about 1 kHz) at a particular range r. Because of the coherent integration, the clutter from signals arriving from other

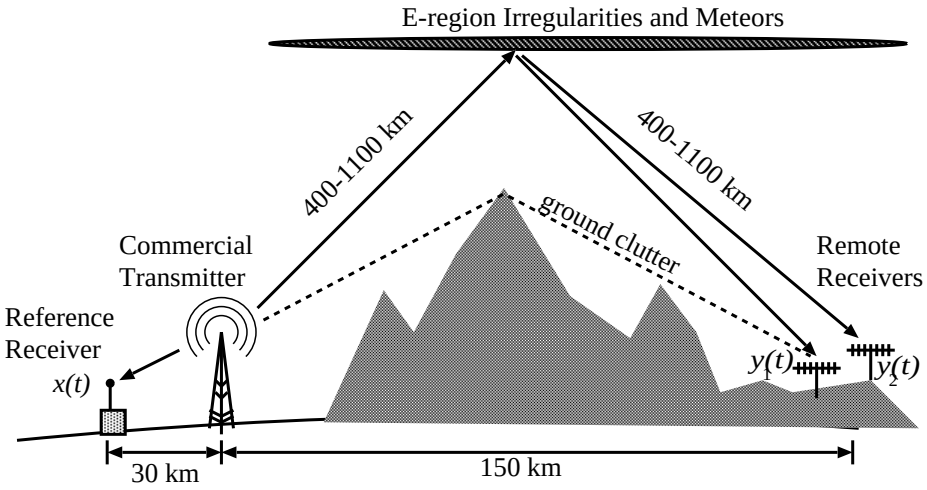

Figure 1: A sketch of the system configuration. The reference receiver supplies a clean copy of the transmitter signal $x(t)$, while the remote receiver is shielded by a mountain range, largely free of direct illumination, and able to collect scattered signal $y(t)$. Auroral and meteor scatter appear at slant ranges out to 1100 km, at altitudes from 85 to 125 km; at larger ranges the E region falls below the line-of-sight horizon.

ranges is greatly reduced; thus, $z_n(r;\bar{t})$ is an unbiased estimate of the scattering voltage. Sequences of $z_n(r;\bar{t})$ may be assembled into time series for conventional FFT-based spectrum estimation:

$$Z_n(r;f) = \mathrm{FFT}_{\bar{t}}\left[z_n(r;\bar{t})\right] \quad (2)$$

$$P(r;f) = \frac{1}{M}\sum_{M}|Z_n(r;f)|^2 \quad (3)$$

Examples of the Doppler power spectrum as a function of range are shown in Fig. 2.

We can immediately form the cross spectrum in the same manner as the Cornell group by correlating voltage spectra from different antennas:

$$P_{nm}(r;f) = \frac{1}{L}\sum_{L} Z_n(r;f)Z_m^*(r;f) \quad (4)$$

Here the sum over L represents a time average of L (sequential) batches of individual spectral estimates. The cross spectrum P_{nm} represents the correlation of the signals arriving with Doppler shift f at each antenna. Because the noise processes polluting the two antennas are uncorrelated, the expected value of $P_{nm}(r;f)$ is zero for ranges and Dopplers in which no echo is present.

If we normalize the cross spectrum by the self power, we have

$$C_{nm}(r;f) = \frac{P_{nm}(r;f)}{\sqrt{P'_{nn}(r;f)P'_{mm}(r;f)}} \quad (5)$$

where $P'_{nn}(r;f) = P_{nn}(r;f) - N_n$, which is to say, the self power on antenna n less the self noise power. The self noise power must be estimated and removed, or the normalized cross-spectrum will be biased (strongly diminished in magnitude), although the phase will be preserved.

In Fig. 3, we illustrate the interferometer phase, cross spectrum magnitude, and self power for the meteor shown in Fig. 2. The data were acquired for 10 seconds, during which the meteor appeared for about 1 second of significant amplitude. The raw data rate is 100 ksamp/sec, with initial decimation of 200, leading to a partially detected time series $z_n(t)$ on each antenna with rate 5000 samples/second. These time series were assembled into 19 256-pt blocks, and on each of the 38 blocks an FFT was performed. Thus, in (4) there were $L = 19$ incoherent averages, leading to an experimental uncertainty of about 20 percent of the magnitude of the power spectra (about 1 dB). It is apparent that the power spectra on each antenna (bottom panel of Fig. 3) are consistent.

The interferometer phase (top panel of Fig. 3) shows a strong concentration over the Doppler bins with large magnitude. In principle, it is possible to estimate the target size from the magnitude of the normalized cross

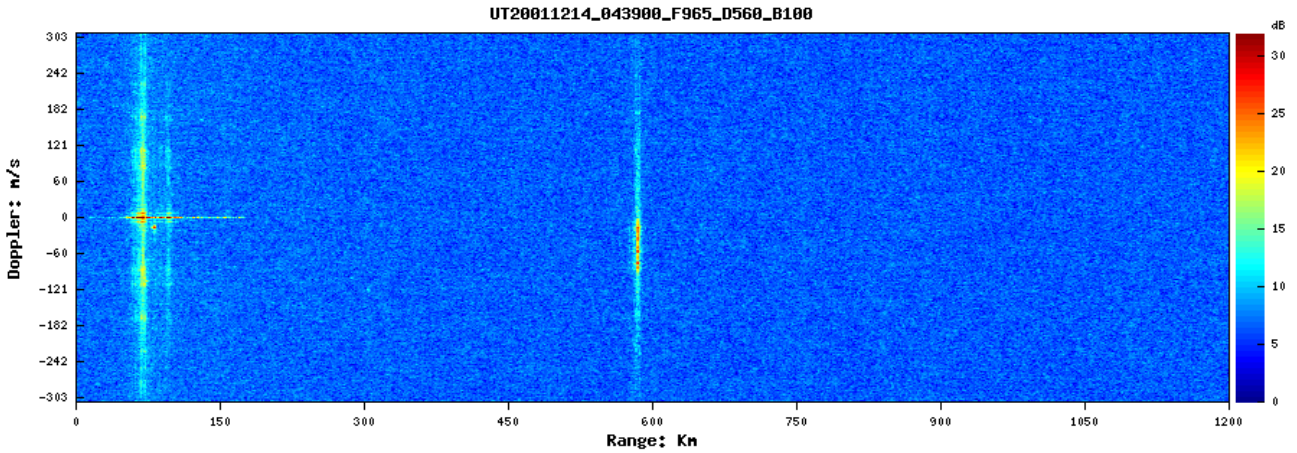

Figure 2: A range-Doppler display from MRR. The horizontal axis is bistatic distance (km), the vertical axis is Doppler velocity (m/s), and the color scale is in dB. The features from 50 - 200 km are ground clutter and aircraft; note the prominent (but low) ambiguity sidelobes of the FM broadcast. A meteor is apparent at 570 km; its Doppler shift indicates significant vertical extent, tracing wind shear at mesosphere altitude.

spectrum (see discussion below), but we can also estimate the size by the standard deviation of the phase estimates. In this case, the standard deviation of the phase estimates over the marked area of concentration is about $\Delta\phi \approx 0.2$ rad. With an antenna baseline of 70 m, $kd \approx 140$; thus, $\Delta\theta \approx \Delta\phi/(kd)$, and the transverse size is $r\Delta\theta \approx 2$ km at $r = 800$ km.

Of course, the interferometer phase varies considerably over the Doppler velocities with significant amplitude. This indicates that the meteor trail is present at several different altitudes, revealing different mesospheric wind velocities (which we expect).

Our interferometer baseline is quite large, so that the interferometer is strongly aliased in angle. From the data above, we have no direct information about the absolute arrival angle; the interferometer lobes are about 3° apart in the direction the antennas are oriented (normal to the interferometer baseline). A shorter baseline will be constructed to remove the azimuth aliasing.

We have observed E region irregularities with the interferometer, but there is no correlation apparent — which simply indicates that the scattering volume exceeds 3° in azimuth (about 35 km at 700 km range).

DISCUSSION

Close observation will reveal that some of the cross-spectral magnitudes exceed unity, an unphysical result which is caused by imperfect removal of the self-noise on each antenna. A second flaw remains in the phase (top panel) of Fig. 3; the phase at Doppler shifts far from the meteor peak is not distributed uniformly over $[-\pi, \pi]$. This is because the ambiguity sidelobes of the meteor reach to Doppler shifts far from the true spectral peak. These Doppler features appear to arise from the same part of the sky, and generate phase similar to that of the meteor peak.

Compact cosmic sources of VHF energy which appear within the field of view of the antennas can in principle generate false interferometric signatures. However, we expect their contribution to be very small for the following reasons:

- The antenna is oriented such that its maximum sensitivity is pointed towards a relatively quiet part of the sky.
- The initial partial correlation step which generates $z_n(r;\bar{t})$ strongly decreases the effective bandwidth of the receiver and thus decreases the quantity of cosmic noise entering the receiver for subsequent processing.
- The long baseline between the reference and scatter antennas assures that there will be vanishing correlation for targets whose size exceeds 20μ radian, or approximately 4 arc seconds.

On the other hand, by performing ordinary radio astronomy observations on the scatter antennas only, we have the interesting possibility of measuring the antenna pattern simultaneously and independently of radar observations.

Figure 3: The interferometer phase, normalized magnitude, and the antenna self powers (dB, arbitrary units) for the meteor shown in Fig. 2. The cross spectrum rises to a large value in the Doppler bins holding the meteor, and the interferometer phase is compact, indicating a small object.

Although the computational burden associated with passive radar is larger than that of conventional radars, the speed of modern desktop computers is adequate for the task. The 0–1200 km range-Doppler profile can be computed in real time with about 4 CPUs in the the 1 GHz class. Computational burden is no longer a challenge for this technique.

SUMMARY

We have presented the first passive VHF radar interferometry observations of ionospheric targets. The data are of high quality, and suggest that passive radar is indeed a potent tool for ionospheric radar remote sensing.

REFERENCES

[1] F. D. Lind, J. D. Sahr, and D. M. Gidner. First passive radar observations of auroral E region irregularities. *Geophys. Res. Lett.*, 26:2155–58, 1999.

[2] J. F. Providakes, D. T. Farley, W. E. Swartz, and D. Riggin. Plasma irregularities associated with a morning discrete auroral arc: Radar interferometer observations and theory. *J. Geophys. Res.*, 90:7513, 1985.

[3] J. D. Sahr and F. D. Lind. The Manastash Ridge Radar: A passive bistatic radar for upper atmospheric radio science. *Radio Sci.*, 32:2345–2358, 1997.

[4] C. Zhou, J. D. Sahr, M. G. Meyer, and D. M. Gidner. Ground clutter subtraction algorithm for vhf passive radar observation of the upper atmosphere. In *2002 URSI General Assembly*, 2002.